

The LAKE model.
Technical description

Victor Stepanenko
Moscow State University

April 5, 2020

Chapter 1

The thermo- and hydrodynamics of the model

1.1 Basics of 1D equations in the water column

Here we present a general 1D modelling framework used in the LAKE model. We start with the general transport Reynolds-averaged equation for the quantity f , that might be one of velocity components, temperature, turbulent kinetic energy (TKE) and other scalars:

$$\frac{\partial f}{\partial t} = -\frac{\partial u_i f}{\partial x_i} - \frac{\partial F_i}{\partial x_i} + R_f, \quad (1.1)$$

assuming mass conservation equation for incompressible fluid:

$$\frac{\partial u_i}{\partial x_i} = 0, \quad (1.2)$$

where u_i is the velocity component along x_i Cartesian axis ($x_3 = z$ being an axis pointing along gravity, $x_1 = x$, $x_2 = y$), F_i is the sum of non-advective fluxes of a property f along x_i , and R_f standing for the sum of sources and sinks of f . Now, introduce the averaging procedure as:

$$\bar{f} = \frac{\int_{A(z)} f dx dy}{A(z)}, \quad (1.3)$$

with $A(z)$ denoting the horizontal cross-section of a lake. After applying this operator to (1.1) and making use of appropriate simplifications we get (for rigorous derivation we refer to Appendix A):

$$\begin{aligned} \frac{\partial A \bar{f}}{\partial t} = & - \int_{\Gamma_{A(z)}} f (\mathbf{u}_h \cdot \mathbf{n}) dl - \frac{\partial A \bar{w} \bar{f}}{\partial z} - \\ & - \frac{\partial A \bar{F}_{nz}}{\partial z} - \frac{\partial A \bar{F}_{tz}^*}{\partial z} + \frac{dA}{dz} [F_{nz,b}(z) + F_{tz,b}(z)] + A \bar{R}_f, \end{aligned} \quad (1.4)$$

where, $\mathbf{u}_h = (u, v) = (u_1, u_2)$, $w = u_3$, \mathbf{n} – outer unit normal to the boundary of $A(z)$, $\bar{F}_{tz}^* = \bar{F}_{tz} + \overline{w' f'}$ – effective horizontally averaged turbulent flux with F_{tz} standing for small-scale (subfilter-scale) flux and w' , f' are deviations of respective variables from horizontal mean; F_{nz} is a non-turbulent flux of variable f , e.g. radiative flux for temperature and bubble flux for dissolved gases, subscript "b" denotes values of variables at the sloping bottom as functions of z . Horizontal averaging of continuity equation leads to:

$$\frac{\partial A \bar{w}}{\partial z} = - \int_{\Gamma_{A(z)}} (\mathbf{u}_h \cdot \mathbf{n}) dl. \quad (1.5)$$

1.1.1 Horizontal averaging

1.1.2 The normalized vertical coordinate

1.2 Thermodynamics of water column

1.3 Dynamics of water column

1.3.1 Governing equations

1.3.2 Parameterization of mean surface level gradient

In order to calculate the mean gradients of the surface level $\overline{\partial h_s / \partial x}$, $\overline{\partial h_s / \partial y}$, we use the following parameterization, based on that originally proposed by U.Svensson (Svensson, 1978).

First, for simplicity we assume the lake's body horizontal cross-section to be an ellipse at all levels. Then, we define South-North (S-N) and West-East (W-E) vertical cross-sections of the lake's body, drawn through the ellipse center (given that the ellipses' centers at all levels fall onto the same vertical line, ref! to figure). Now, we denote the horizontal width of the S-N cross-section as $L_{S-N}(z)$, and define $L_{W-E}(z)$ analogously. The mass flux through the W-E section increases the lake surface level in the Northern half of a lake, and decreases it in the Southern part. The same holds for Western and Eastern parts. This means, that we can write

$$\frac{dh_N}{dt} A_0(t) = -\frac{dh_S}{dt} A_0(t) = 2 \int_0^1 v L_{W-E} h d\xi, \quad (1.6)$$

$$\frac{dh_E}{dt} A_0(t) = -\frac{dh_W}{dt} A_0(t) = 2 \int_0^1 u L_{S-N} h d\xi, \quad (1.7)$$

where we introduced h_S, h_N, h_W and h_E as the average deviations of the lake surface level in Southern, Northern, Western and Eastern halves of the lake surface, respectively, and $A_0(t)$ is the lake surface area. In the above equations we assumed that the deviations h_* are small, so that the use of $A_0(t)$ instead of $A_0(h_*, t)$ is justified.

Once h_* are found, we parameterize the needed surface level gradients as:

$$g \frac{\partial h_s}{\partial x} \approx \frac{g\pi^2}{4} \frac{h_E - h_W}{L_{W-E,0}}, \quad (1.8)$$

$$g \frac{\partial h_s}{\partial y} \approx \frac{g\pi^2}{4} \frac{h_N - h_S}{L_{S-N,0}}. \quad (1.9)$$

It can be shown (ref!) that this parameterization of seiches exactly fits the analytical solution for specific case of 1D channel flow oscillations described by shallow water equations (Merian formula). To implement the above equations we need $L_{W-E}(z)$, $L_{S-N}(z)$ for each particular lake to be simulated. These parameters are easily derived from $A(z)$, given the each lake horizontal cross-section is an ellipse, and its eccentricity is known (making the model cross-section shape to be close to the cross-section of a real lake).

1.4 Turbulent mixing

1.5 Thermodynamics of ice

1.6 Thermodynamics of snow

Ice cover acts in winter as a heat insulating layer and thereby controls the growth and melting of ice cover. Hence, the heat transport in a snow cover should be well reproduced. In order to achieve realistic results on snow temperature and depth, a number of processes are included in the model, snow gravitational compaction and liquid water transport, among others. The mathematical description of these processes closely follows the formulation from (Volodina et al., 2000) (for liquid water equation derivation see Appendix B). The governing equations have a form:

$$c_{sn}\rho_{sn}\frac{\partial T}{\partial t} = \frac{\partial}{\partial z}\lambda_{sn}\frac{\partial T}{\partial z} + \rho_{sn}L_{fr}F_{fr}, \quad (1.10)$$

$$\frac{\partial W}{\partial t} = -(1-W)\frac{\rho_{w0}}{\rho_{sn}}\frac{\partial \gamma_v}{\partial z} - F_{fr} - \frac{W}{\rho_{sn}}C_{sn}. \quad (1.11)$$

Here, the snow thermal conductivity is calculated by the empirical formula:

$$\lambda_{sn} = C_1 \left(\frac{\rho_{sn}}{\rho_{w0}} \right)^4 + C_2 \frac{\rho_{sn}}{\rho_{w0}} + C_3, \quad (1.12)$$

with $C_1 = 2.514$, $C_2 = 0.796$, $C_3 = 0.021$, $[C_*] = J/(m * s * K)$ ¹. The specific heat is determined by liquid water content:

$$c_{sn} = Wc_w + (1-W)c_i. \quad (1.13)$$

The rate of phase transition, F_{fr} , is non-zero, when the temperature crosses the melting point for water, and is calculated according to heat balance in a given numerical cell. The gravitational flux of liquid water, m/s, is given by:

$$\gamma_v = h_c \left(\frac{W_v - W_{hc}}{p - W_{hc}} \right)^3, \quad (1.14)$$

where $W_v = W\rho_{sn}\rho_{w0}^{-1}$ is a volumetric ratio of liquid water. The snow compaction term, C_{sn} , enters the equation for ρ_{sn} :

$$\frac{\partial \rho_{sn}}{\partial t} = -\rho_{w0}\frac{\partial \gamma_v}{\partial z} + C_{sn}. \quad (1.15)$$

Boundary condition at the top of snow is a heat balance equation, including heat and radiation fluxes. The bottom boundary conditions, i.e. the condition at the snow-ice interface is continuity of heat flux and temperature. For liquid water content, the gravitational flux is zero at the bottom (boundary condition for the top is not needed, as (1.11) is a 1-st order equation).

1.7 Thermodynamics of bottom sediments (ground)

¹Hereafter, if not otherwise stated, * in the subscript means all possible values of the subscript in the current context

Chapter 2

Biochemistry in the water column and sediments

2.1 Governing equations for dissolved gases and organic carbon in a water column

The dynamics of three dissolved gases is considered: methane (CH_4), oxygen (O_2) and carbon dioxide (CO_2). However, dissolved carbon dioxide is supposed to be always in carbonate equilibrium, so that it enters concentration of dissolved inorganic carbon (DIC), $C_{DIC} = C_{CO_2} + C_{HCO_3^-} + C_{CO_3^{2-}}$, and it is the change of DIC that reflects the number of carbon atoms in CO_2 molecules added to (or lost by) a solution from (to) atmosphere, bubbles, respiring organisms or decaying organical matter (see Section 2.2).

In addition, dissolved organic carbon (DOC), particulate organic carbon (both living, POCL, and dead, POCD) are calculated. POCL includes phytoplankton and zooplankton.

The species listed above obey the following equation system:

$$\frac{\partial C_{CH_4}}{\partial t} = \mathcal{A}_{CH_4}^\pm + \text{Adv}_A(C_{CH_4}) + \text{Dif}_A(C_{CH_4}) + B_{CH_4} - O_{CH_4}, \quad (2.1)$$

$$\frac{\partial C_{O_2}}{\partial t} = \mathcal{A}_{O_2}^\pm + \text{Adv}_A(C_{O_2}) + \text{Dif}_A(C_{O_2}) + B_{O_2} + P_{O_2} - R_{O_2} - D_{O_2} - S_{O_2} - O_{O_2}, \quad (2.2)$$

$$\frac{\partial C_{DIC}}{\partial t} = \mathcal{A}_{DIC}^\pm + \text{Adv}_A(C_{DIC}) + \text{Dif}_A(C_{DIC}) + B_{CO_2} - P_{CO_2} + R_{CO_2} + D_{CO_2} + S_{CO_2} + O_{CO_2}, \quad (2.3)$$

$$\frac{\partial C_{DIP}}{\partial t} = \mathcal{A}_{DIP}^- + \text{Adv}_A(C_{DIP}) + \text{Dif}_A(C_{DIP}) + D_{DIP} + R_{DIP} + S_{DIP} - P_{DIP}, \quad (2.4)$$

$$\frac{\partial \rho_{DOC,au}}{\partial t} = \mathcal{A}_{DOC,au}^- + \text{Adv}_A(\rho_{DOC,au}) + \text{Dif}(\rho_{DOC,au}) + E_{POCL} - D_{DOC,au}, \quad (2.5)$$

$$\frac{\partial \rho_{DOC,al}}{\partial t} = \mathcal{A}_{DOC,al}^\pm + \text{Adv}_A(\rho_{DOC,al}) + \text{Dif}(\rho_{DOC,al}) - D_{DOC,al}, \quad (2.6)$$

$$\frac{\partial \rho_{POCL}}{\partial t} = \mathcal{A}_{POCL}^\pm + \text{Adv}_A(\rho_{POCL}) + \text{Dif}(\rho_{POCL}) + P_{POCL} - R_{POCL} - E_{POCL} - D_{h,POCL}, \quad (2.7)$$

$$\frac{\partial \rho_{POCD}}{\partial t} = \mathcal{A}_{POCD}^- + \text{Adv}_A(\rho_{POCD}) - \frac{1}{h} \frac{\partial(w_g \rho_{POCD})}{\partial \xi} + \text{Dif}(\rho_{POCD}) - D_{POCD} + D_{h,POCL}. \quad (2.8)$$

where $\text{Dif}_A(\bullet) \equiv M(\xi, t) \frac{\partial \bullet}{\partial \xi} + \frac{1}{Ah^2} \frac{\partial}{\partial \xi} \left(Ak_s \frac{\partial \bullet}{\partial \xi} \right)$, $\text{Dif}(\bullet) \equiv M(\xi, t) \frac{\partial \bullet}{\partial \xi} + \frac{1}{h^2} \frac{\partial}{\partial \xi} \left(k_s \frac{\partial \bullet}{\partial \xi} \right)$, $\text{Adv}_A(\bullet) = -\frac{1}{Ah} \frac{\partial(Aw\bullet)}{\partial \xi}$ – vertical advection, $M(\xi, t) = \left(\frac{\xi}{h} \frac{dh}{dt} - \frac{r-E}{h} \right)$ is a metric term arising from using

the normalized vertical coordinate originating at moving water surface, w_g is a sedimentation velocity of POCD particles. Equations (2.5)-(2.8) do not contain A , i.e. they are not horizontally-averaged (see Appendix A) but 1D equations, where horizontal homogeneity of computed variable is assumed. This is caused by uncertainty how to assess marginal flux of these substances at the sloping sediments-water interface. The r.h.s of these equations represent diffusion (assuming $k_s = k_{s,t} + k_{s,m}$ with the same eddy diffusivity $k_{s,t}$ and molecular diffusivity $k_{s,m}$ for all species; molecular diffusivity is not included in POCL and POCD equations), sources and sinks due to the following processes:

- dissolution/exsolution of gases at the bubble-water interface (B_{CH_4} , B_{O_2} and B_{CO_2});
- photosynthesis (P_{O_2} , P_{CO_2} , P_{POCL} , P_{DIP});
- respiration (R_{O_2} , R_{CO_2} , R_{POCL} , R_{DIP});
- biochemical oxygen demand in the water column (D_{O_2} , D_{CO_2} , D_{DOC} , D_{POCD});
- sedimentary oxygen demand (S_{O_2} , S_{CO_2} , S_{DIP});
- methane aerobic oxidation in the water column (O_{CH_4} , O_{O_2} , O_{CO_2});
- death of living species ($D_{h,POCL}$)

All variables in the above list are positive definite, excepting B_{CH_4} , B_{O_2} and B_{CO_2} that may be either positive or negative. All concentrations in (2.1)-(2.4) are expressed in mol/m^3 that allows for simple relations of sinks/sources in different equations based on stoichiometry of the respective reactions. Organic carbon variables DOC, POCL and POCD in (2.5)-(2.8) are molar concentrations of carbon atoms contained in these organic groups. Terms B_{CO_2} , P_{CO_2} , R_{CO_2} , D_{CO_2} , S_{CO_2} , O_{CO_2} in (2.3) possess " CO_2 " subscript because carbon atoms are supplied to or removed from DIC of a solution in a form of CO_2 .

Terms \mathcal{A}_*^* stand for input and output of respective species to a lake by inlets and outlets, respectively; " \pm " sign in uppercase means, that both tributaries and effluents are taken into account, "-" indicates that only effluents are included.

We note that equations (2.1)-(2.3) and (2.4)-(2.8) may form a coupled system if sinks/sources at the r.h.s. are related, or be solved as independent subsets otherwise. The details will be given below.

In the following sections we first consider carbonate equilibrium, then continue with boundary conditions for (2.1)-(2.3) and finally describe the abovementioned sources/sinks in more detail. The formulations for photosynthesis, respiration, biochemical oxygen demand and sedimentary oxygen demand basically follow (Stefan and Fang, 1994) and (Hanson et al., 2004).

2.2 Carbonate equilibrium

Carbonate equilibrium means the equilibrium in the following reactions:



Involving kinetic constants of these reactions yields, that the DIC

$$C_{DIC} \equiv C_{CO_2} + C_{HCO_3^-} + C_{CO_3^{2-}} = C_{CO_2} [1 + k_1 10^{pH} + k_1 k_2 10^{2pH}]. \quad (2.11)$$

Here, the constants are given by Arrhenius equation:

$$k_i = k_{i0} \exp \left[-\frac{E_{act,i}}{R} \left(\frac{1}{T} - \frac{1}{T_0} \right) \right], \quad i = 1, 2, \quad (2.12)$$

R – universal gas constant, $k_1 = 4.3 * 10^{-7} \text{ mol/l}$, $k_2 = 4.7 * 10^{-11} \text{ mol/l}$, $E_{act,1} = 7.66 * 10^3 \text{ J/mol}$, $E_{act,2} = 1.49 * 10^4 \text{ J/mol}$. Thus, C_{CO_2} is readily calculated given C_{DIC} value, and vice versa.

Carbon atoms are added or removed from carbonate equilibrium system in a form of CO_2 during respiration, photosynthesis and organic chemical and physical processes, hence the change of C_{DIC} equals to number of CO_2 consumed or produced. This explains the sense of terms in equation (2.3). For obtaining CO_2 flux across bubble surface or CO_2 diffusive flux to the atmosphere, C_{CO_2} is needed and is calculated from (2.11).

2.3 Boundary conditions for dissolved gases in a water column

The top boundary condition (at the lake-atmosphere interface) for any dissolved gas concentration for the case of open water has the form:

$$\left. \frac{k_s}{h} \frac{\partial C}{\partial \xi} \right|_{\xi=0} = F_C, \quad (2.13)$$

where C is C_{CH_4} , C_{O_2} or C_{CO_2} , and F_C is the diffusive flux of a gas into the atmosphere, positive upwards. This flux is calculated according to the widely used parameterization:

$$F_C = k_{ge}(C|_{\xi=0} - C_{ae}), \quad (2.14)$$

with C_{ae} being the concentration of the gas in water equilibrated with the atmospheric concentration and described by Henry law and $k_{ge}, m/s$ denoting the gas exchange coefficient, the so-called "piston velocity". The latter is written as:

$$k_{ge} = k_{600} \sqrt{\frac{600}{Sc(T)}}, \quad (2.15)$$

with the Schmidt number $Sc(T)$ having individual values for different gases and being temperature-dependent (ref!). The k_{600} coefficient has been a subject of numerous studies, and a number of concepts have been proposed to quantify it (Donelan et al., 2002). We adopt two widespread options for k_{600} : (i) empirical dependence on wind speed and (ii) surface renewal model.

The dependency on wind velocity takes the form (Cole and Caraco, 1998):

$$k_{600} = C_{k_{600},1} + C_{k_{600},2} |\mathbf{u}_{a,10}|^{n_{k_{600}}}. \quad (2.16)$$

Here, $\mathbf{u}_{a,10}$ stands for the wind speed at 10 m above the surface. The simple empirical eq. (2.16) "integrates" the effects of wind speed on a number of processes such as turbulence in adjacent layers of water and air, wave development and breaking, cool skin dynamics, and therefore is likely to be not enough sophisticated to express adequately a wide variety of conditions on real lakes. Therefore, we also included surface renewal model (MacIntyre et al., 2010; Heiskanen et al., 2014), that in terms of k_{600} states that:

$$k_{600} = \frac{C_{1,SR}(\epsilon|_{\xi=0}\nu_w)^{\frac{1}{4}}}{\sqrt{600}}, \quad (2.17)$$

where ν_w designates molecular viscosity of water. As TKE dissipation rate is available directly from $k - \epsilon$ closure, we do not use any special parameterization for $\epsilon|_{\xi=0}$ (e.g., (MacIntyre et al., 2010)).

When a lake is covered by ice, $F_C = 0$, neglecting contribution of diffusion through ice cracks.

The boundary conditions for methane at the sediments-water body interface are:

$$-\frac{k_s}{h} \frac{\partial C}{\partial \xi} \Big|_{\xi=1} = -k_{s,s} \frac{\partial C_s}{\partial z_s} \Big|_{z_s=0}, \quad (2.18)$$

$$C|_{\xi=1} = \left(\frac{C_s}{p} \right) \Big|_{z_s=0}. \quad (2.19)$$

Here, additional subscript "s" denotes characteristics of sediments. Porosity appears in (2.19) because C_s is a bulk concentration in soil. These relations mean continuity of both diffusive flux and concentration at the water-sediments boundary.

Table 2.1: Constants for water-air gas exchange

Constant	Variable in the code	Units	Value
$C_{k_{600},1}$	constvel1	m/s	$5.75 * 10^{-6}$
$C_{k_{600},2}$	constvel2	$(m/s)^{1-n_{k_{600}}}$	$5.97 * 10^{-7}$
$n_{k_{600}}$	wind10power	n/d	1.7
$C_{1,SR}$	c1	n/d	0.5

2.4 Dissolution/exsolution of gases at the bubble-water interface

2.4.1 Bubble model

The bubble model presented here closely follows that described in (McGinnis et al., 2006). Consider the evolution of a bubble, consisting of a gas mixture, rising from a lake bottom. In this case the quantity of each i -th gas in the bubble M_i (mol) is changing due to dissolution into oceanic water according to equation

$$\frac{dM_i}{dt} = v_b \frac{dM_i}{dZ} = -4\pi r_b^2 K_i (H_i(T) P_i - C_i), i = 1, \dots, n_g, \quad (2.20)$$

where r_b is the bubble radius (m), H_i - the Henry constant dependent on temperature T (K), P_i the partial pressure of i -th gas (Pa), C_i is the concentration of a gas dissolved in water (mol/m^3), K_i is exchange coefficient, v_b is bubble vertical velocity (m/s), Z is the vertical coordinate originating at the bottom and pointing opposite to gravity (m), n_g is the number of gases in a mixture. Five gases are considered simultaneously in a bubble: methane, carbon dioxide, oxygen, nitrogen and argon. The temperature in the bubble is assumed to be equal to temperature of environment lake water at the depth of current bubble location. It means that the heat exchange between the rising bubble and water is assumed to be intensive enough to dominate over the adiabatic cooling of the bubble. This is likely to be a rough approximation,

however, including adiabatic bubble temperature change would increase the complexity of the model. The temperature dependency of Henry constants for flat solute surface is taken from (Sander, 1999). The effect of gas-water interface curvature on equilibrium gas pressure is omitted because when using Thomson formula it turns to be negligible as long as typical bubble radiuses in lakes and ocean are considered ($\geq 1 \text{ mm}$). Exchange coefficient K_i is dependent on molecular diffusivity in water, bubble radius and its velocity according to empirical formulae from (Zheng and Yapa, 2002). The bubble velocity is determined from equilibrium between buoyancy force and environment resistance defined by quadratic law for small radiuses ($r_b < 1.3 \text{ mm}$) and taking into account bubble surface oscillations for larger sizes (Jamialahmadi et al., 1994).

For each component of gas mixture one applies an ideal gas law because under the typical pressures at small depths (e.g. several dozens of meters) Van der Waals forces are small:

$$\frac{4}{3}P_i\pi r_b^3 = M_iRT, i = 1, \dots, n_g, \quad (2.21)$$

where R is the universal gas constant. The surface tension pressure is small for the bubbles with radiuses typical for lacustrine and marine environments. Then, when equating the gas mixture pressure $\sum_{i=1}^{n_g} P_i$ to hydrostatic pressure at a given depth $p_a + \rho_{w0}g(h - Z)$ (ρ_{w0} being the mean density of water and p_a the atmospheric pressure) and using (2.21) one yields:

$$r_b = \left[\frac{3RT \sum_{i=1}^{n_g} M_i}{4\pi(p_a + \rho_{w0}g(h - Z))} \right]^{1/3}. \quad (2.22)$$

For solution of $2n_g + 1$ equations (2.20)-(2.22) the boundary conditions are needed. These are initial gases' quantities $M_{i,Z=0} = M_{i0}(t), i = 1, \dots, n_g$, that are the quantities when the bubble crosses the lake bottom. In the model they are initialized as follows:

$$M_0 = \frac{\frac{4}{3}\pi r_{b0}^3(p_a + \rho_{w0}gh)}{R T|_{Z=0}}, \quad (2.23)$$

$$M_{i0} = \alpha_i M_0, i = 1, \dots, n_g,$$

where M_0 - is the total gas quantity in the bubble (mols). From (2.23) it is seen that bubble initialization is given by initial bubble radius r_{b0} and molar fractions of mixture components α_i . The bubble model described above is numerically solved by Euler explicit scheme.

2.4.2 Interaction between bubbles and dissolved gases

To calculate B_i , $B_1 = B_{CH_4}$, $B_2 = B_{CO_2}$, $B_3 = B_{O_2}$ (see (2.1)-(2.3)) in our model we consider an idealized situation when all bubbles rising from the bottom have the same initial radius r_{b0} and identical gas composition. From (2.20)-(2.22) it immediately follows that their radius and composition are the same at any depth ξ . Since the vertical gas transport by bubbles changes with depth only due to exchange with water solution, one writes

$$B_i = + \frac{1}{h} \frac{\partial F_{B,i}}{\partial \xi}. \quad (2.24)$$

Here $F_{B,i}$ is the bubble gas flux ($\text{mol}/(\text{m}^2\text{s})$) pointed upwards (this leads to "+" sign in the r.h.s.). The definition of this flux is

$$F_{B,i} = M_i n_b v_b. \quad (2.25)$$

We introduced bubble concentration (m^{-3}) here. All bubbles release at the bottom and completely dissolve simultaneously at some depth or reach the surface. Moreover, it is known (Yamamoto et al., 2009; McGinnis et al., 2006) that bubbles with diameter $\approx 1 \text{ mm}$ are unstable and split up. Hence, in the model it is assumed that a bubble with $r_b \geq 0.5 \text{ cm}$ splits into two. In the depth interval between two subsequent bubble splits the bubble flux (that is the number of bubbles crossing the horizontal surface of 1 m^2 per second) is constant, and at the depth of division it doubles. One may rewrite (2.24) as follows

$$B_i = \frac{1}{h} \frac{\partial(n_b v_b M_i)}{\partial \xi} = \frac{F_{B0,i}}{h} \frac{\partial(N m_i)}{\partial \xi}, \quad (2.26)$$

where we have introduced the relative bubble flux $N m_i$ with $m_i = \frac{M_i}{M_{i0}}$, $N = \frac{n_b v_b}{n_{b0} v_{b0}}$, and $F_{B0,i}$ is the bottom bubble flux (zero subscript indicates the bottom value of a variable). Evidently, $N(\xi) = 2^k$, k being the number of bubble divisions happened below the depth ξ . If the bottom bubble flux of one gas is known (in this model it is methane, $i = 1$) then the bottom fluxes of other gases are determined by bottom bubble composition:

$$F_{B0,i} = F_{B0,1} \frac{\alpha_i}{\alpha_1}, i = 2, \dots, n_g. \quad (2.27)$$

2.5 Photosynthesis

The intensity of photosynthesis in terms of oxygen production is expressed as (ref!):

$$P_{O_2} = \frac{P_{max} L_{min} L_P \rho_{Chl-a}}{H_{sec} \mu_{O_2}}. \quad (2.28)$$

The denominator here serves to convert units in the r.h.s. from $\text{mg}/(\text{l} * \text{h})$ to $\text{mol}/(\text{m}^3 \text{s})$. The P_{max} value expresses limitation of oxygen production by temperature in a form:

$$P_{max} = C_P \theta_P^{(T-T_0)}, \quad (2.29)$$

so that C_P is P_{max} at the reference temperature $T = T_0$. The effect of soluble reactive phosphorus is postulated by Michaelis-Menten equation:

$$L_P = \frac{C_{DIP}}{K_{hs,DIP,Chla} + C_{DIP}}. \quad (2.30)$$

The limitation of oxygen production by the available photosynthetically active radiation PAR (S_{PAR}) is given by the following Haldane kinetics:

$$L_{min} = \frac{S_{PAR}(1 + 2\sqrt{C_{Lmin,1}/C_{Lmin,2}})}{S_{PAR} + C_{Lmin,1} + S_{PAR}^2/C_{Lmin,2}}. \quad (2.31)$$

The PAR intensity delivering maximum to L_{min} ($=1$) is $S_{PAR} = \sqrt{C_{Lmin,1} C_{Lmin,2}}$. In the model, these coefficients are specified as (Stefan and Fang, 1994; Megard et al., 1984):

$$C_{Lmin,1} = C_{PAR} \theta_{PAR}^{(T-T_0)}, \quad (2.32)$$

$$C_{Lmin,2} = H(T - T_{00}) C_{Lmin,2,>T_{00}} + [1 - H(T - T_{00})] C_{Lmin,2,<T_{00}}, \quad (2.33)$$

with $H(\bullet)$ being a Heavyside function, and T_{00} is another reference temperature. It is seen from (2.31), that $L_{min} \rightarrow 0$ if $S_{PAR} \rightarrow 0$ and $S_{PAR} \rightarrow \infty$, i.e. PAR inhibits photosynthesis at both low and high values of its intensity. To calculate S_{PAR} , it is assumed that the ratio

of PAR intensity to total shortwave radiation intensity in the water column, α_{PAR} , is known, thereby

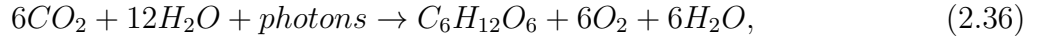
$$S_{PAR} = \alpha_{PAR} H_{sec} T_{J \rightarrow Eins} S. \quad (2.34)$$

The coefficient transforming from J to *Einstein* (Einstein is an energy of Avogadro number of photons), $T_{J \rightarrow Eins}$, is calculated in approximation of uniform distribution of energy in PAR region, yielding

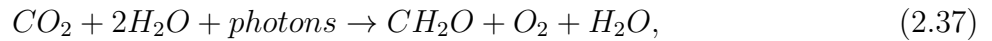
$$T_{J \rightarrow Eins} = \frac{\lambda_{PAR}}{N_A h_P c}, \quad (2.35)$$

with N_A, h_P, c denoting Avogadro number, Planck constant and the light speed in vacuum, respectively, all in SI units.

Finally, from the gross photosynthesis reaction:



or, in a shortened form:



we see that the carbon dioxide consumption equals oxygen production, i.e. $P_{CO_2} = P_{O_2}$.

Table 2.2: Constants in photosynthesis model

Constant	Variable in the code	Units	Value
C_P	c1_pmax	h^{-1}	9.6
θ_P	c2_pmax	n/d	1.036
T_0	T_0	$^{\circ}C$	20
T_{00}	T_00	$^{\circ}C$	10
μ_{O_2}	molmass_o2	g/mol	32
H_{sec}	hour_sec	s	3600
C_{PAR}	k1_c1	$Einstein/(m^2 * h)$	0.687
θ_{PAR}	k1_c2	n/d	1.086
$C_{Lmin,2,>T_{00}}$	k2_c2	$Einstein/(m^2 * h)$	15.
$C_{Lmin,2,<T_{00}}$	k2_c1	$Einstein/(m^2 * h)$	5.
λ_{PAR}	lambda_PAR0	m	$5.5 * 10^{-7}$ (550 nm)
α_{PAR}	short2PAR	n/d	0.48
$K_{hs,DIP,Chla}$	halfsat_DIP_photosynt	mol/m^3	$10^{-3}/\mu_p$, $[\mu_p]=g/mol$

Equation (2.36) also implies that $P_{POCL} = P_{CO_2}$.

2.6 Respiration

2.6.1 Formulation by Stefan and Fang

Respiration is a process opposite to photosynthesis. In the model, the oxygen consumption due to respiration is given by:

$$R_{O_2} = \frac{k_r \theta_r^{T-T_0} \rho_{Chl-a}}{Y_{CHO_2} D_{sec} \mu_{O_2}}, \quad (2.38)$$

where Y_{CHO2} is a mass ratio of chlorophyll-a to oxygen, utilized in respiration. Analogously to the case of photosynthesis, $R_{CO_2} = R_{O_2}$.

Table 2.3: Constants in respiration model

Constant	Variable in the code	Units	Value
Y_{CHO2}	YCHO2	mg/mg	$8 * 10^{-3}$
k_r	k_r	day^{-1}	$1 * 10^{-1}$
θ_r	theta_r	n/d	1.045
D_{sec}	day_sec	s	86400
μ_{O_2}	molmass_o2	g/mol	32

2.6.2 Formulation by Hanson et al.

P.Hanson et al. (Hanson et al., 2004) assume, that respiration is performed by "living particles", POCL, only in epilimnion, and may be scaled by gross primary production (i.e., photosynthesis rate), $R_{POCL} = \alpha_{POCL} P_{POCL}$, $\alpha_{POCL} = 0.8$. In contrast, we assume that this process happens at all depths where enough oxygen *in situ* is available, with the same scaling. Evidently,

$$R_{O_2} = R_{CO_2} = \alpha_{POCL} P_{POCL}. \quad (2.39)$$

2.7 Biochemical oxygen demand (BOD)

2.7.1 Formulation by Stefan and Fang

Biochemical oxygen demand is an oxygen consumption due to organic matter decomposition in the water column. It is expressed as (Stefan and Fang, 1994):

$$B_{O_2} = \frac{k_b \theta_b^{T-T_0} \rho_{Chl-a} C_{st}}{D_{sec} \mu_{O_2}}. \quad (2.40)$$

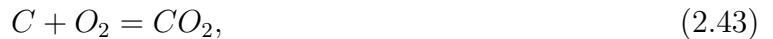
Here, temperature dependence constant is given by:

$$\theta_b = [\theta_{b1} H(T - T_0) + \theta_{b2} [1 - H(T - T_0)]] H(T - T_{md}). \quad (2.41)$$

This means switching between constants θ_{b1} and θ_{b2} at the reference temperature T_0 and "switching off" BOD below the temperature of maximum density, T_{md} , implying ice-cover conditions. The constant C_{st} reflects the stoichiometry of respective reactions. According to (Stefan and Fang, 1994), it reads:

$$C_{st} = M_{O_2/C} M_{C/Chl}, \quad (2.42)$$

where $M_{O_2/C}$ is the mass ratio of oxygen to carbon in the aerobic organic decay reaction:



and $M_{C/Chl}$ is a mass ratio of carbon to chlorophyll-a in the organic matter. The equation (2.43) shows that $D_{CO_2} = D_{O_2}$.

Table 2.4: Constants in biochemical oxygen demand model

Constant	Variable in the code	Units	Value
k_b	k_b	day^{-1}	0.1
θ_{b1}	theta_b1	n/d	1.047
θ_{b2}	theta_b2	n/d	1.13
T_{md}	T_md	$^{\circ}C$	4.
$M_{O_2/C}$	mO2C_dec	mg/mg	8/3
$M_{C/Chl}$	mCChla_dec	mg/mg	30.

2.7.2 Formulation by Hanson et al.

Here, for biochemical oxygen demand, we adopt respiration terms, related to dead organic particles (POCD) and dissolved organic carbon (DOC) from (Hanson et al., 2004), namely, D_{POCD} and D_{DOC} in our notation. P.Hanson et al. suggest that $D_{POCD} = \rho_{POCD}/\tau_{POCD}$, $D_{DOC} = \rho_{DOC}/\tau_{DOC}$ with time scales $\tau_{POCD} = 20D_{sec}$, $\tau_{DOC} = 200D_{sec}$. We extend this model to distinguish between allochthonous and autochthonous DOC, so that:

$$D_{O_2} = D_{CO_2} = \left(\frac{\rho_{POCD}}{\tau_{POCD}} + \frac{\rho_{DOC,au}}{\tau_{DOC,au}} + \frac{\rho_{DOC,al}}{\tau_{DOC,al}} \right). \quad (2.44)$$

In current model version, a default option is $\tau_{DOC,au} = \tau_{DOC,al} = \tau_{DOC}$, however, $\tau_{DOC,au}$ and $\tau_{DOC,al}$ may be adjusted, and generally $\tau_{DOC,al} > \tau_{DOC,au}$.

2.7.3 Photodissociation of DOC

Photodissociation of DOC means removal of C atoms from DOM to DIC. A formula presented in (Fichot and Miller, 2010; Koehler et al., 2014) can be readily extended to a case where optic properties of water medium vary with depth:

$$P_{d,DOC} = \int_{\lambda_{min}}^{\lambda_{max}} \alpha_{CDOM}(\lambda, z) E(\lambda, 0) \exp \left(- \int_0^z \alpha(\lambda, z') dz' \right) \Phi(\lambda) d\lambda, \quad (2.45)$$

where ...

2.8 Sedimentary oxygen demand (SOD)

Two sedimentary oxygen demand formulations are implemented in the model. In both of them, the sedimentary oxygen demand appears as a sink in (2.2) and in essence is the contribution of the vertical flux at the lake's bottom to the horizontally averaged oxygen concentration:

$$S_{O_2} = - \frac{F_{SOD}}{Ah} \frac{\partial A}{\partial \xi}. \quad (2.46)$$

In the first SOD formulation which is that used in (Stefan and Fang, 1994), the bottom oxygen flux due to organics decomposition is a function of temperature only:

$$F_{SOD} = \frac{1}{D_{sec} \mu_{O_2} 10^3} S_{b20} \theta_s^{T-T_0}. \quad (2.47)$$

Here, again switching between two different values of temperature dependence parameter, θ_s , is used:

$$\theta_s = \theta_{s1}H(T - T_0) + \theta_{s2}[1 - H(T - T_0)]. \quad (2.48)$$

This parameterization does not include dependence of SOD on oxygen concentration, hence the O_2 uptake in sediments is not zero even when $C_{O_2} = 0$. From this point the more physically grounded SOD parameterization is the model provided by Robert Walker and William Snodgrass (Walker and Snodgrass, 1986). Basing on the argument that SOD is contributed both by diffusion (governed by Fickian law) and biochemical consumption (described by Michaelis-Menten kinetics), they derive:

$$F_{SOD} = \mu_\beta \frac{C_{O_2}}{k_{O_2,SOD} + C_{O_2}} + k_c C_{O_2}, \quad (2.49)$$

where μ_β is proportional to organics oxidation potential rate in sediments, and k_c is the mass transfer coefficient. Both are thought to be exponentially dependent on temperature:

$$\mu_\beta = \mu_{\beta,0} \theta_{\mu_\beta}^{T-T_{\mu_\beta}}, k_c = k_{c,0} \theta_{k_c}^{T-T_{k_c}}. \quad (2.50)$$

The stoichiometry of SOD is assumed to be close to that of BOD (2.43), therefore, $S_{CO_2} = S_{O_2}$. Additionally, the flux of O_2 due to SOD at the lake bottom, F_{SOD} , is used as the bottom (lake deepest point) boundary condition for the oxygen equation (2.2).

Table 2.5: Constants in sedimentary oxygen demand model

Constant	Variable in the code	Units	Value
S_{b20}	Sb20	$mg/(m^2 day)$	10^3
θ_{s1}	theta.s1	n/d	1.065
θ_{s2}	theta.s2	n/d	1.13
θ_{μ_β}	thetamu.SOD	n/d	1.085
θ_{k_c}	thetaC_SOD	n/d	1.103
T_{μ_β}	-	K	25
T_{k_c}	-	K	20
$\mu_{\beta,0}$	mubeta0	$mol/(m^2 * s)$	$0.5/(\mu_{O_2} D_{sec}), [\mu_{O_2}] = g/mol$
$k_{c,0}$	kc0	m/s	$0.045/D_{sec}$

2.9 Exudates and death rate of POCL

Hanson et al. suggest exudation to be scaled with photosynthesis rate, $E_{POCL} = \beta_{POCL} P_{POCL}$, $\beta_{POCL} = 0.03$ and the death rate to be defined as $D_{h,POCL} = \frac{\rho_{POCL}}{\tau_{Dh}}$, where time scale τ_{Dh} ranges from $1.1D_{sec}$ in hypolimnion to $33D_{sec}$ in epilimnion.

2.10 Dissolved inorganic phosphorus

Dissolved inorganic phosphorus or soluble reactive phosphorus gets P atoms from degradation of organic matter (dissolved organic compounds, sediments and dead organisms), respiration, and

looses them during buildup of living organisms, i.e. photosynthesis. The respective sinks and sources in equation (2.4) are set proportional to carbon exchange rates via P/C stoichiometric ratios:

$$D_{DIP} = \gamma_{P/C,DOM,au} D_{DOC,au} + \gamma_{P/C,DOM,al} D_{DOC,al} + \gamma_{P/C,POM} D_{POCD}, \quad (2.51)$$

$$R_{DIP} = \gamma_{P/C,POM} R_{CO_2}, \quad (2.52)$$

$$P_{DIP} = \gamma_{P/C,POM} P_{CO_2}, \quad (2.53)$$

$$S_{DIP} = \gamma_{P/C,SOD} S_{CO_2}. \quad (2.54)$$

Here, parameters γ_* are ratios of P to C atoms in dissolved organic and particulate organic matter.

Table 2.6: Constants in dissolved inorganic phosphorus model

Constant	Variable in the code	Units	Value
$\gamma_{P/C,DOM,au}$	DOMauto_PtoC	n/d	1/106
$\gamma_{P/C,DOM,al}$	DOMallo_PtoC	n/d	1/199
$\gamma_{P/C,POM}$	POM_PtoC	n/d	1/106
$\gamma_{P/C,SOD}$	sedoxid_PtoC	n/d	1/106

2.11 Sedimentation of organic particles

In the current model version we use the Stokes sedimentation velocity below the mixed layer:

$$w_s = \frac{4}{3A} \frac{\Delta g d^2}{\nu_m}, \quad (2.55)$$

and the high-Reynolds-number limit of this variable

$$w_s = \sqrt{\frac{4}{3B} \Delta g d} \quad (2.56)$$

in the mixed layer. Here, $\Delta = \rho_p / \rho_{w0} - 1$, ρ_p is a particle's density, and d – its diameter, the typical values for constants may be chosen as $A = 30.0$, and $B = 1.25$ (Song et al., 2008), and the density of organic particles as 1.25 g/cm^3 (Avnimelech et al., 2001).

2.12 Chlorophyll-a dynamics

2.12.1 Formulation by Stefan and Fang

The chlorophyll-a dynamics in the model follows a simple scheme suggested in (Stefan and Fang, 1994), where chlorophyll-a density is calculated as:

$$\rho_{Chl-a} = \rho_{Chl-a,0} H(H_a - z), \quad (2.57)$$

where the active layer, H_a , is a maximum value between mixed-layer depth, H_{ML} , and the photic zone depth, H_{PZ} . The mixed-layer depth is defined as the depth of maximum Brunt-Väisälä frequency, and the photic zone depth is estimated as the depth at which the PAR

irradiance drops to 10% of its surface value. The mean chlorophyll-a concentration, $\rho_{Chl-a,0}$, is assigned according to a trophic status of the lake: $2 * 10^{-3} \text{ mg/l}$ for oligotrophic lakes, $6 * 10^{-3} \text{ mg/l}$ for mesotrophic lakes and $15 * 10^{-3} \text{ mg/l}$ for eutrophic lakes. In turn, the trophic status is formally defined from the water turbidity. The Secchi disk values of 2 m and 3.5 m are used to distinguish between eutrophic and mesotrophic, mesotrophic and oligotrophic states, respectively. These thresholds are expressed in the model through light extinction coefficient values, α , using Poole and Atkins formula (Poole and Atkins, 2009):

$$\alpha = \frac{k_{PA}}{z_{SD}}, \quad (2.58)$$

where z_{SD} is the Secchi disk depth and $k_{PA} = 1.7$. The above chlorophyll-a scheme is identical to that of (Stefan and Fang, 1994), excepting for it does not take into account the annual cycle of $\rho_{Chl-a,0}$.

2.12.2 Chlorophyll model based on light and phosphorus limitation

This approach follows (Sadeghian et al., 2018) and (Chapra, 2008). Introduce a fraction of chlorophyll-a mass in total phytoplankton mass, $\gamma_{Chl/phyto}$. Assuming that photoplankton comprises most of POCL, yields:

$$\gamma_{Chl/phyto} = \frac{\rho_{Chl-a}}{\rho_{POCL} \times \mu_{CH_2O}}. \quad (2.59)$$

This fraction is controlled by availability of nutrients (phosphorus and nitrogen) and light (PAR). Assuming nitrogen is non-limiting, allows to neglect its content and consider the following approximation:

$$\gamma_{Chl/phyto} = \gamma_{Chl/phyto,0} + \gamma_{Chl/phyto,1} \times L_P(C_{DIP})(1 - \Phi_{PAR}(S_{PAR})), \quad (2.60)$$

where $\gamma_{Chl/phyto,0}$ and $\gamma_{Chl/phyto,1}$ are constants. The effect of soluble reactive phosphorus (term L_P) is given by Michaelis-Menten equation (2.30).

There are two options of quantifying the influence of PAR on chlorophyll-a fraction. The first one is to assume $\Phi_{PAR} = L_{min}$, where L_{min} is given by (2.31). The second one is to use the relation (Sadeghian et al., 2018):

$$\Phi_{PAR}(S_{PAR}) = \frac{S_{PAR}}{S_{PAR,MP}} \exp \left(1 - \frac{S_{PAR}}{S_{PAR,MP}} \right), \quad (2.61)$$

where $S_{PAR,MP}$ is PAR intensity, optimal for photosynthesis. Thus, at each time and depth, ρ_{Chl-a} is diagnosed using POCL, DIP and PAR quantities.

The constants of chlorophyll-a model described above are given in the following table.

Table 2.7: Constants of Chlorophyll-a model

Constant	Variable in the code	Units	Value
$\gamma_{Chl/phyto,0}$	C1_Chla_to_POCLphyto	n/d	$6.4 * 10^{-3}$
$\gamma_{Chl/phyto,1}$	C2_Chla_to_POCLphyto	n/d	$4.5 * 10^{-2}$
$S_{PAR,MP}$	PAR_prod_max_warm	Einstein/(m ² *h)	$\sqrt{C_{Lmin,1} C_{Lmin,2}}$

2.13 Aerobic methane oxidation

The aerobic oxidation of methane follows the equation:



that means $O_{O_2} = 2O_{CO_2} = 2O_{CH_4}$. To calculate O_{CH_4} , three options are available in the model. The simplest one is the first-order kinetics:

$$O_{CH_4} = k_{ox,CH_4} C_{CH_4}, \quad (2.63)$$

where k_{ox,CH_4} is a constant (according to (Striegl et al., 1998), is chosen $0.38D_{sec}^{-1}s^{-1}$).

More sophisticated, but containing 4 constants, Michaelis-Menten kinetics, has the general form:

$$O_{CH_4} = V_{max} \exp \left[\frac{\Delta E_{ox,CH_4}}{R} \left(\frac{1}{T} - \frac{1}{T_0} \right) \right] \frac{C_{CH_4}}{K_{hs,CH_4} + C_{CH_4}} \frac{C_{O_2}}{K_{hs,O_2} + C_{O_2}}, \quad (2.64)$$

where we introduce the activation energy of methane oxidation reaction, $\Delta E_{ox,CH_4}$, reaction potential V_{max} at the reference temperature, T_0 , half-saturation constants K_{hs,CH_4} , K_{hs,O_2} . However, a number of studies (Utsumi et al., 1998; Liikanen et al., 2002a; Striegl et al., 1998) have shown a weak dependence of reaction potential on temperature. Hence, the second option in the model is the Michaelis-Menten kinetics (2.64) without exponential term.

In a case of oxygen depletion aerobic methane oxidation should approach zero in the water column, so that O_2 should be kept in (2.64). Unfortunately, we have found a quite limited data on K_{hs,O_2} in the literature. However, from the experience on methane modeling in wetlands (Watson et al., 1997) and measurements in the lake sediments (Lidstrom and Somers, 1984) $K_{hs,O_2} \approx K_{hs,CH_4}$, and we have used this approximation in our model.

In order to avoid dependency of methane oxidation on oxygen concentration the third option considers simplified Michaelis-Menten equation, formally coming from (2.64) for highly oxygenated waters:

$$O_{CH_4} = V_{max} \frac{C_{CH_4}}{K_{hs,CH_4} + C_{CH_4}}. \quad (2.65)$$

The Michaelis-Menten constants are given in the table 2.8.

Table 2.8: Michaelis-Menten kinetics constants for methane oxidation in the water column

Reference	V_{max}	K_{hs,CH_4}	Remarks
(Lidstrom and Somers, 1984)	3.8 $10^{-2} H_{sec}^{-1} \text{ mol}/(m^3 s)$	*	$9.5 \pm 1.2 \text{ mol}/m^3$ Measured in top 1 cm of bottom sediments
(Liikanen et al., 2002a)	3.6 $10^{-2} D_{sec}^{-1} \text{ mol}/(m^3 s)$	*	$5.5 * 10^{-3} \text{ mol}/m^3$ shallow profundal water, 4 m
(Liikanen et al., 2002a)	1.4 $10^{-1} D_{sec}^{-1} \text{ mol}/(m^3 s)$	*	$4.4 * 10^{-2} \text{ mol}/m^3$ deep profundal water, 9 m

2.14 Methane dynamics in the bottom sediments

2.14.1 Governing equation

The dynamics of bulk methane concentration (the number of dissolved molecules in moles per unit volume of sediment / soil) is governed by three processes: production, ebullition and diffusion:

$$\frac{\partial C_{CH_4}}{\partial t} = \frac{\partial}{\partial z_s} \left(k_{CH_4} \frac{\partial C_{CH_4}}{\partial z_s} \right) + P_{soil,CH_4} - E_{soil,CH_4} - O_{soil,CH_4}, \quad (2.66)$$

where z_s is a downward coordinate originating at the sediments' surface, P_{soil,CH_4} and E_{soil,CH_4} are the methane production and ebullition rates, respectively, and O_{soil,CH_4} is the aerobic methane oxidation, all positive. Aerobic methane oxidation term is non-zero only in the top thin computational layer; in the rest layers oxygen is assumed to be depleted, that is the well-known observational fact (Huttunen et al., 2006). Note, that the methane concentration C_{CH_4} accounts for dissolved gas only, so that ebullition rate is a sink term for it. The soil diffusion coefficient is given by:

$$k_{CH_4} = C_{tort} k_{CH_4,w}, \quad (2.67)$$

and molecular diffusivity for methane dissolved in water, $k_{CH_4,w}$, depends on temperature according to quadratic function. Here, C_{tort} is a tortuosity coefficient (set to 0.66), accounting for tortuosity of diffusion paths through soil skeleton.

The eq. (2.66) should also contain the plant-mediated transport of methane for vegetated lakes. In future we intend to include this mechanism in the model.

2.14.2 Production

Methane production is comprised of two sources (Stepanenko et al., 2011). First is methane production from decomposition of "young" organics, i.e. the current NPP of lake ecosystem, depositing at the lake bottom. The organic material reaching the bottom after coast abrasion also contributes to this source, located at the top of sediments. The second source of methane is to be switched on in the model for thermokarst lakes for which it is known, that the "old" organics, sequestered in the premafrost below the talik, is subjected to biotic degradation when the temperature exceeds the melting point in the process of talik deepening (Walter et al., 2007). Thus, this second source has its maximum in the vicinity of talik bottom.

Formulations for both production sources base at the assumption that the production is proportional to quantity and quality of organics, exponentially dependent on temperature and does not happen under temperatures less than melting point:

$$P_{soil,CH_4,i} \propto \rho_{org,i} H(T - T_{mp}) q_{10}^{T/10} (1 + \alpha_{O_2,inhib} C_{O_2})^{-1} [1 - H(C_{SO_4} - C_{SO_4,crit})], \quad i = old, new \quad (2.68)$$

where T_{mp} standing for the melting point temperature, q_{10} is times that the methane production increases when the temperature rises by 10°C, and $\alpha_{O_2,inhib}$ denoting the constant for methanogenesis inhibition by oxygen. Oxygen concentration, C_{O_2} , decays very fast within a few millimeters below the bottom (Huttunen et al., 2006). The last multiplier in (2.68) represents suppression of methanogenic *Archaea* by sulfate-reducing bacteria when sulfate concentration exceeds critical value, $C_{SO_4,crit}$ (Lovley and Klug, 1986). The constant of proportionality in (2.68) should reflect the quality of the organic substrate regarding methane production. The density (kg/m^3) of organics available for anaerobic decomposition resulting in methane production, $\rho_{org,i}$, may be estimated from either 1st-order or Michaelis-Menten kinetics. For young

organics we adopt an assumption $\rho_{org,new} \propto \exp(-\alpha_{new}z_s)$ (Walter and Heimann, 2000), that formally can be derived from 1st-order kinetics for $\rho_{org,new}$ decay and constant rate of depositing new sediments at the lake bottom. For the old organics content, an expression is developed in (Stepanenکو et al., 2011) based on Michaelis-Menten decomposition rate for $\rho_{org,old}$:

$$\rho_{org,old} = \rho_{org,old,0} \left[2 + \lambda_\rho - \sqrt{(1 + \lambda_\rho)^2 + \gamma_\rho(h_t^2 - z_s^2)} \right], \quad (2.69)$$

where $\lambda_\rho = \rho_{org,old,0}K_{org,old}^{-1}$, $\gamma_\rho = 2VK_{org,old}^{-1}C_t^{-2}$ are the derived constants, and the original constants are given in the Table 2.9, h_t - talik depth. Thus, basing on (2.69), we get:

$$P_{soil,CH_4,i} = P_{i,0}\rho_i^*H(T - T_{mp})q_{10}^{T/10}(1 + \alpha_{O_2,inhib}C_{O_2})^{-1} \quad (2.70)$$

$$\rho_i^* = \begin{cases} \exp(-\alpha_{new}z_s) & : i = new \\ \left[2 + \lambda_\rho - \sqrt{(1 + \lambda_\rho)^2 + \gamma_\rho(h_t^2 - z_s^2)} \right] & : i = old \end{cases}$$

Here, $P_{new,0}, P_{old,0}$ are new constants to be calibrated.

Table 2.9: Constants for methane production in the lake sediments

Constant	Variable in the code	Units	Value (reference)
$\rho_{org,old,0}$ (the density of old organics below the talik)	C0_oldorg	kg/m^3	18
$K_{org,old}$ (the half-saturation constant of Michaelis-Menten decomposition of old organics in talik)	k_oldorg	kg/m^3	$3 * 10^{-1}$
V (the maximum decomposition rate of old organics in talik)	V_oldorg	$kg/(m^3 * yr)$	$2 * 10^{-3}$
C_t (a constant in a talik deepening law, $h_t = C_t\sqrt{t}$, t - time)	$ms^{-1/2}$	C_talik_age	0.5 (West and Plug, 2008)
q_{10}	q100	n/d	2.3 (Liikanen et al., 2002b)
α_{new}	lambda_new_org	m^{-1}	3

2.14.3 Ebullition

The formation of bubbles (ebullition) happens in the model only in the sediments layer, as we haven't found evidences in literature that this process occurs at significant rates in the water column. As the bubble formation takes a certain amount of methane from the dissolved state,

it is represented by a sink term in (2.66). The rate of this sink is determined by a methane concentration excess over a critical value, $C_{CH_4,crit}$:

$$E_{soil,CH_4} = r_{ebul} H(C_{CH_4} - C_{CH_4,crit}) (1 - H(w_i)) (C_{CH_4} - C_{CH_4,crit}), \quad (2.71)$$

where we also postulated that ebullition happens in non-frozen soils only, and $r_{ebul} = 1.0 H_{sec}^{-1}$ (Walter and Heimann, 2000). Now, the critical concentration of dissolved methane in soil, $C_{CH_4,crit}$, is assumed to be a fraction, $r_{crc} = 0.4$, of saturation concentration ((Wania, 2007) and references therein). In turn, the saturation concentration is found from two conditions: (i) the sum of partial pressures of all gases comprising a bubble equilibrates the external hydrostatic load, $P = g(\rho_{w0}h + \rho_s z_s)$, and (ii) partial pressure of each gas is in equilibrium with the dissolved gas according to Henry's law (with Henry constants $H_*(T)$, * standing for the gas name). We assume the presence of two dissolved gases in sediments, entering the bubble composition: nitrogen and methane. Thus, the critical bulk methane concentration is expressed as:

$$C_{CH_4,crit} = r_{crc} p \left(P H_{CH_4}(T) - \frac{H_{CH_4}(T)}{H_{N_2}(T)} C_{N_2} \right), \quad (2.72)$$

with p standing for sediments' porosity. Following (Bazhin, 2001) we assume that nitrogen rapidly decays to zero in the top thin sediments layer, and therefore contributes to (2.72) only in the top numerical layer of the in-sediments' grid.

The mechanical interaction of bubbles with the soil skeleton (Scandella et al., 2011) is omitted in the current version of the model, and it is assumed that all bubbles generated at different depths in the bottom sediments instantly reach the lake's bottom. Therefore, the methane bubble flux at the lake bottom is:

$$F_{CH_4,b}(\xi = 1) = \int_0^d E_{soil,CH_4} dz_s, \quad (2.73)$$

where d is the thickness of ground domain in the model.

2.14.4 Aerobic methane oxidation in bottom sediments

Chapter 3

List of symbols

Symbol	Name	Variable in the code	Units
General			
h	Lake depth	h1, h2	m
l	Ice thickness	l1, l2	m
h_{sn}	Snow thickness	hs1	m
$\xi = \frac{z}{h}$	Normalized vertical coordinate	dzeta	n/d
Snow cover			
W	Liquid water content in snow	-	kg/kg
Biochemistry			
ρ_{Chl-a}	Chlorophyll-a density in a water column	Chl.a	mg/l
S_{PAR}	The intensity of photosynthetically active radiation	PAR	$Einstein/(m^2 * h)$

Bibliography

- Yoram Avnimelech, Gad Ritvo, Leon E. Meijer, and Kochba Malka. Water content, organic carbon and dry bulk density in flooded sediments. *Aquacultural Engineering*, 25:25–33, 2001.
- N.M. Bazhin. Gas transport in a residual layer of a water basin. *Chemosphere - Global Change Science*, 3(1):33 – 40, 2001. ISSN 1465-9972. doi: [http://dx.doi.org/10.1016/S1465-9972\(00\)00041-6](http://dx.doi.org/10.1016/S1465-9972(00)00041-6). URL <http://www.sciencedirect.com/science/article/pii/S1465997200000416>.
- Steven C. Chapra. *Surface water-quality modeling*. Waveland Pr Inc, 2008. ISBN 978-1577666059.
- Jonathan J Cole and Nina F Caraco. Atmospheric exchange of carbon dioxide in a low-wind oligotrophic lake measured by the addition of SF₆. *Li*, 43(4):647–656, 1998. doi: 10.4319/lo.1998.43.4.0647.
- M. A. Donelan, W. M. Drennan, E. S. Saltzman, and R. Wanninkhof, editors. *Gas Transfer at Water Surfaces*. Geophysical Monograph Series. American Geophysical Union, Washington, D. C., January 2002. ISBN 9781118668634. doi: 10.1029/GM127. URL <http://doi.wiley.com/10.1029/GM127>.
- Cédric G Fichot and William L Miller. An approach to quantify depth-resolved marine photochemical fluxes using remote sensing: Application to carbon monoxide (CO) photoproduction. *Remote Sensing of Environment*, 114(7):1363–1377, 2010. ISSN 0034-4257. doi: <https://doi.org/10.1016/j.rse.2010.01.019>. URL <http://www.sciencedirect.com/science/article/pii/S0034425710000507>.
- Paul C. Hanson, Amina I. Pollard, Darren L. Bade, Katie Predick, Stephen R. Carpenter, and Jonathan A. Foley. A model of carbon evasion and sedimentation in temperate lakes. *Global Change Biology*, 10(8):1285–1298, 2004. ISSN 13541013. doi: 10.1111/j.1529-8817.2003.00805.x. URL <http://doi.wiley.com/10.1111/j.1529-8817.2003.00805.x>.
- JOUNI J. Heiskanen, IVAN Mammarella, SAMI Haapanala, JUKKA Pumpanen, TIMO Vesala, SALLY MacIntyre, and ANNE Ojala. Effects of cooling and internal wave motions on gas transfer coefficients in a boreal lake. *Tellus B*, 66, May 2014. ISSN 1600-0889. doi: 10.3402/tellusb.v66.22827. URL <http://www.tellusb.net/index.php/tellusb/article/view/22827/xml>.
- J T Huttunen, T S Väisänen, S K Hellsten, and P J Martikainen. Methane fluxes at the sediment-water interface in some boreal lakes and reservoirs. *Boreal Env. Res.*, 11:27–34, 2006.
- M. Jamialahmadi, C. Branch, and J. Müller-Steinhagen. Terminal bubble rise velocity in liquids. *Trans. Inst. Chem. Eng.*, 72:119–122, 1994.

- Birgit Koehler, Tomas Landelius, Gesa A Weyhenmeyer, Nanako Machida, and Lars J Tranvik. Sunlight-induced carbon dioxide emissions from inland waters. *Global Biogeochemical Cycles*, 28(7):696–711, 2014. doi: 10.1002/2014GB004850. URL <https://agupubs.onlinelibrary.wiley.com/doi/abs/10.1002/2014GB004850>.
- M E Lidstrom and L Somers. Seasonal study of methane oxidation in lake washington. *Applied and environmental microbiology*, 47(6):1255–60, June 1984. ISSN 0099-2240. URL <http://www.pubmedcentral.nih.gov/articlerender.fcgi?artid=240212&tool=pmcentrez&rendertype=abstract>.
- A. Liikanen, J. T. Huttunen, K. Valli, and P. J. Martikainen. Methane cycling in the sediment and water column of mid-boreal hyper-eutrophic Lake Kevaton, Finland. *ARCHIV FUR HYDROBIOLOGIE*, 154(4):585–603, 2002a.
- Anu Liikanen, Timo Murtoniemi, Heikki Tanskanen, Tero Väisänen, and Pertti J. Martikainen. Effects of temperature and oxygen availability on greenhouse gas and nutrient dynamics in sediment of a eutrophic mid-boreal lake. *Biogeochemistry*, 59(3):269–286, 2002b. ISSN 0168-2563. doi: 10.1023/A:1016015526712. URL <http://dx.doi.org/10.1023/A%3A1016015526712>.
- Derek R. Lovley and Michael J. Klug. Model for the distribution of sulfate reduction and methanogenesis in freshwater sediments. *Geochimica et Cosmochimica Acta*, 50(1):11–18, January 1986. ISSN 00167037. doi: 10.1016/0016-7037(86)90043-8. URL <http://www.sciencedirect.com/science/article/pii/0016703786900438>.
- Sally MacIntyre, Anders Jonsson, Mats Jansson, Jan Aberg, Damon E. Turney, and Scott D. Miller. Buoyancy flux, turbulence, and the gas transfer coefficient in a stratified lake. *Geophysical Research Letters*, 37(24):n/a–n/a, December 2010. ISSN 00948276. doi: 10.1029/2010GL044164. URL <http://doi.wiley.com/10.1029/2010GL044164>.
- D. F. McGinnis, J. Greinert, Y. Artemov, S. E. Beaubien, and A. West. Fate of rising methane bubbles in stratified waters: How much methane reaches the atmosphere? *Journal of Geophysical Research: Oceans*, 111(C9):n/a–n/a, 2006. ISSN 2156-2202. doi: 10.1029/2005JC003183. URL <http://dx.doi.org/10.1029/2005JC003183>.
- R O Megard, D W Tonkyn, and W H Senft. Kinetics of oxygenic photosynthesis in planktonic algae. *Journal of Plankton Research*, 6(2):325–337, 1984. doi: 10.1093/plankt/6.2.325. URL <http://plankt.oxfordjournals.org/content/6/2/325.abstract>.
- H. H. Poole and W. R. G. Atkins. Photo-electric Measurements of Submarine Illumination throughout the Year. *Journal of the Marine Biological Association of the United Kingdom*, 16(01):297, May 2009. ISSN 0025-3154. doi: 10.1017/S0025315400029829. URL http://journals.cambridge.org/abstract_S0025315400029829.
- Amir Sadeghian, Steven C. Chapra, Jeff Hudson, Howard Wheeler, and Karl-Erich Lindenschmidt. Improving in-lake water quality modeling using variable chlorophyll a/algal biomass ratios. *Environmental Modelling & Software*, 101:73–85, mar 2018. ISSN 1364-8152. doi: 10.1016/J.ENVSOFT.2017.12.009. URL <https://www.sciencedirect.com/science/article/pii/S1364815217306953>.
- Rolf Sander. Compilation of henry’s law constants for inorganic and organic species of potential importance in environmental chemistry, 1999.

- Benjamin P Scandella, Charuleka Varadharajan, Harold F Hemond, Carolyn Ruppel, and Ruben Juanes. A conduit dilation model of methane venting from lake sediments. *Geophysical Research Letters*, 38(6):n/a—n/a, 2011. ISSN 1944-8007. doi: 10.1029/2011GL046768. URL <http://dx.doi.org/10.1029/2011GL046768>.
- Zhiyao Song, Tingting Wu, Fumin Xu, and Ruijie Li. A simple formula for predicting settling velocity of sediment particles. *Water Science and Engineering*, 1(1):37–43, 2008. doi: 10.3882/j.issn.1674-2370.2008.01.005.
- Heinz G Stefan and Xing Fang. Dissolved oxygen model for regional lake analysis. *Ecological Modelling*, 71(13):37–68, 1994. ISSN 0304-3800. doi: [http://dx.doi.org/10.1016/0304-3800\(94\)90075-2](http://dx.doi.org/10.1016/0304-3800(94)90075-2). URL <http://www.sciencedirect.com/science/article/pii/0304380094900752>.
- V.M. Stepanenko, E.E. Machulskaya, M.V. Glagolev, and V.N. Lykosov. Numerical modeling of methane emissions from lakes in the permafrost zone. *Izv. AN. Fiz. Atmos. Ok*, 47(2): 275–288, 2011. doi: 10.1134/S0001433811020113.
- Robert G Striegl, Catherine M Michmerhuizen, and U S Geological Survey. Hydrologic influence on methane and carbon dioxide dynamics at two north-central Minnesota lakes. *Limnol. Oceanogr.*, 43(7):1519–1529, 1998.
- U. Svensson. *A mathematical model of the seasonal thermocline*. Phd, Lund Inst. of Technol., 1978.
- Motoo Utsumi, Nojiri Yulihiko, Takeshi Nakamura, Takeshi Nozawa, Akira Otsuki, and Humitake Seki. Oxidation of dissolved methane in a eutrophic, shallow lake: Lake Kasumigaura, Japan. *Limnol. Oceanogr.*, 43(3):471–480, 1998.
- E. Volodina, L. Bengtsson, and V.N. Lykosov. Parameterization of heat and moisture transfer in a snow cover for modelling of seasonal variations of land hydrological cycle. *Russian Journal of Meteorology and Climatology*, –(5):5–14, 2000. ISSN 0130-2906.
- Robert R. Walker and William J. Snodgrass. Model for Sediment Oxygen Demand in Lakes. *Journal of Environmental Engineering*, 112(1):25–43, February 1986. ISSN 0733-9372. doi: 10.1061/(ASCE)0733-9372(1986)112:1(25). URL [http://ascelibrary.org/doi/abs/10.1061/\(ASCE\)0733-9372\(1986\)112:1\(25\)](http://ascelibrary.org/doi/abs/10.1061/(ASCE)0733-9372(1986)112:1(25)).
- Bernadette P. Walter and Martin Heimann. A process-based, climate-sensitive model to derive methane emissions from natural wetlands: Application to five wetland sites, sensitivity to model parameters, and climate. *Global Biogeochemical Cycles*, 14(3):745–765, 2000. ISSN 1944-9224. doi: 10.1029/1999GB001204. URL <http://dx.doi.org/10.1029/1999GB001204>.
- Katey M Walter, Laurence C Smith, and F Stuart Chapin. Methane bubbling from northern lakes: present and future contributions to the global methane budget. *Philosophical Transactions of the Royal Society A: Mathematical, Physical and Engineering Sciences*, 365(1856):1657–1676, 2007. doi: 10.1098/rsta.2007.2036. URL <http://rsta.royalsocietypublishing.org/content/365/1856/1657.abstract>.
- R Wania. Modelling northern peatland land surface processes, vegetation dynamics and methane emissions. *University of Bristol PhD Thesis*, 2007.

- Andrea Watson, Karl D. Stephen, David B. Nedwell, and Jonathan R.M. Arah. Oxidation of methane in peat: Kinetics of CH₄ and O₂ removal and the role of plant roots. *Soil Biology and Biochemistry*, 29(8):1257–1267, August 1997. ISSN 00380717. doi: 10.1016/S0038-0717(97)00016-3. URL <http://linkinghub.elsevier.com/retrieve/pii/S0038071797000163>.
- J. J. West and L. J. Plug. Time-dependent morphology of thaw lakes and taliks in deep and shallow ground ice. *Journal of Geophysical Research: Earth Surface*, 113(F1):n/a–n/a, 2008. ISSN 2156-2202. doi: 10.1029/2006JF000696. URL <http://dx.doi.org/10.1029/2006JF000696>.
- A. Yamamoto, Y. Yamanaka, E. Tajika, and E. Tajika A. Yamamoto, Y. Yamanaka. Modeling of methane bubbles released from large sea-floor area: Condition required for methane emission to the atmosphere. *Earth and Planetary Science Letters*, 2009. doi: 10.1016/j.epsl.2009.05.026.
- Li Zheng and Poojitha D Yapa. Modeling gas dissolution in deepwater oil/gas spills. *Journal of Marine Systems*, 31(4):299 – 309, 2002. ISSN 0924-7963. doi: [http://dx.doi.org/10.1016/S0924-7963\(01\)00067-7](http://dx.doi.org/10.1016/S0924-7963(01)00067-7). URL <http://www.sciencedirect.com/science/article/pii/S0924796301000677>.

Appendix A

Equation for horizontally averaged quantity in a lake

Consider equation (1.1) and an auxiliary operator:

$$\tilde{f} = \int_{A(z)} f dx dy. \quad (\text{A.1})$$

The cross-section of a lake with notations used in this derivation is given at Fig. ??.

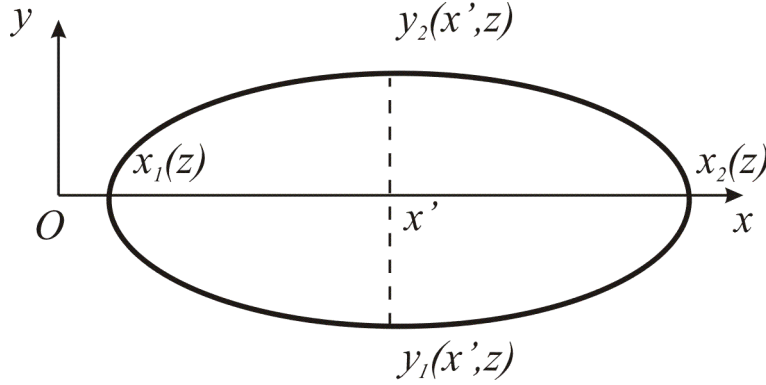


Figure A.1: A lake horizontal cross-section

The integration operator (A.1) possesses the following property:

$$\frac{\partial \tilde{f}}{\partial z} = \widetilde{\frac{\partial f}{\partial z}} + B_f, \quad (\text{A.2})$$

$$B_f = \int_{x_1(z)}^{x_2(z)} \left[\frac{\partial y_2}{\partial z} f(x, y_2, z) - \frac{\partial y_1}{\partial z} f(x, y_1, z) \right] dx, \quad (\text{A.3})$$

stemming from the Leibnitz integral rule. Now let's apply operator $\widetilde{(\dots)}$ to (1.1), then insert $\bar{f} = A\tilde{f}$, and it will lead us to

$$\frac{\partial A\bar{f}}{\partial t} = - \int_{\Gamma_{A(z)}} f(\mathbf{u}_h \cdot \mathbf{n}) dl - \int_{\Gamma_{A(z)}} (\mathbf{F}_h \cdot \mathbf{n}) dl - \frac{\partial A\bar{w}f}{\partial z} - \frac{\partial A\bar{F}_z}{\partial z} + B_{wf} + B_{F_z} + A\bar{R}_f, \quad (\text{A.4})$$

where we introduced $\mathbf{u}_h = \{u_1, u_2\}$ and $\mathbf{F}_h = \{F_1, F_2\}$, and $\Gamma_{A(z)}$ is a boundary of A at depth z . The first term to the right hand side of (A.4) is a horizontal advection of property f through boundaries of a water basin, i.e. the inflow from inlets, outflow by outlets and groundwater

discharge. The second term represents non-advective horizontal fluxes at the lake margins, whereas B_* quantifies the effect of vertical fluxes at the lake bottom of depth z ; we refer to them as to *marginal fluxes*. Equation (A.4) is the most general equation, that is, however, difficult to implement without further simplifications. First, assume that the lake bottom is quasi-horizontal, and in this case the rigid boundary condition for velocity brings $w \approx 0$, $B_{wf} \approx 0$. Then, we suppose that $\mathbf{F} = \{F_1, F_2, F_3\}$ is normal to the bottom boundary, and it is true for diffusive transport, because it is proportional to a gradient of f , and this gradient is usually oriented almost perpendicular to the bottom surface. Therefore, $F_1 \approx 0$, $F_2 \approx 0$, vanishing the second term to the right hand side of (A.4). We also can decompose the vertical advection as $\overline{wf} = \overline{w}\overline{f} + \overline{w'f'}$, $w' = w - \overline{w}$, $f' = f - \overline{f}$. After these modifications, (A.4) devolves to:

$$\frac{\partial A\overline{f}}{\partial t} = - \int_{\Gamma_{A(z)}} f(\mathbf{u}_h \cdot \mathbf{n})dl - \frac{\partial A\overline{w}\overline{f}}{\partial z} - \frac{\partial A\overline{w'f'}}{\partial z} - \frac{\partial A\overline{F_z}}{\partial z} + B_{F_z} + A\overline{R_f}. \quad (\text{A.5})$$

At this stage it is timely to distinguish between turbulent and non-turbulent flux, namely $F_z = F_{tz} + F_{nz}$, and define "effective" turbulent flux, $\overline{F_{tz}^*} = \overline{F_{tz}} + \overline{w'f'}$. This effective turbulent flux includes horizontally-averaged small-scale turbulent flux ($\overline{F_{tz}}$) and the flux mediated by organized flow structures, $\overline{w'f'}$. We also assume that the total non-advective flux F_z at the bottom is the same at all bottom locations of the depth z . Then, taking into account the above hypotheses and

$$B_1 = \int_{x_1(z)}^{x_2(z)} \left[\frac{\partial y_2}{\partial z} - \frac{\partial y_1}{\partial z} \right] dx = \frac{dA}{dz}, \quad (\text{A.6})$$

we transform (A.5) to

$$\frac{\partial A\overline{f}}{\partial t} = - \int_{\Gamma_{A(z)}} f(\mathbf{u}_h \cdot \mathbf{n})dl - \frac{\partial A\overline{w}\overline{f}}{\partial z} - \frac{\partial A\overline{F_{nz}}}{\partial z} - \frac{\partial A\overline{F_{tz}^*}}{\partial z} + \frac{dA}{dz}(F_{nz,b}(z) + F_{tz,b}(z)) + A\overline{R_f}, \quad (\text{A.7})$$

where $F_{*,b}(z)$ denote bottom values of fluxes at depth z . The mean vertical velocity, w , may be expressed from the horizontally integrated continuity equation (1.2):

$$\frac{\partial A\overline{w}}{\partial z} = B_w - \int_{\Gamma_{A(z)}} (\mathbf{u}_h \cdot \mathbf{n})dl, \quad (\text{A.8})$$

where $B_w \approx 0$ according to assumption of quasi-horizontal bottom. This means, w arises from disbalance between inflows and outflows and subsequent water level change. For the LAKE model hasn't been applied for water bodies with significant water level change, the term with w is omitted in (A.9) in the model equation set. The next strong assumptions applied to deliver a familiar 1D lake model equation from (A.9) are:

- the non-turbulent flux, that is the shortwave radiation flux if f is a temperature, is horizontally uniform, so that $\overline{F_{nz}(z)} = F_{nz,b}(z) = F_{nz}(z)$;
- the 'effective' turbulent flux may be represented via the gradient of mean quantity: $\overline{F_{tz}^*} = -k_{eff} \frac{\partial \overline{f}}{\partial z}$;
- the source averaged horizontally, $\overline{R_f(f, \dots)}$, may be approximated as the same function of mean values, $\overline{R_f(f, \dots)} = R_f(\overline{f}, \dots)$.

Substituting these statements into (A.9), we finally get:

$$\frac{\partial \overline{f}}{\partial t} = -\frac{1}{A} \int_{\Gamma_{A(z)}} f(\mathbf{u}_h \cdot \mathbf{n})dl + \frac{1}{A} \frac{\partial}{\partial z} \left(A k_{eff} \frac{\partial \overline{f}}{\partial z} \right) - \frac{1}{A} \frac{\partial A F_{nz}}{\partial z} + \frac{1}{A} \frac{dA}{dz} (F_{nz}(z) + F_{tz,b}(z)) + \overline{R_f}. \quad (\text{A.9})$$

Appendix B

Liquid water equations for snow cover

In the model, liquid water content, W , is expressed as the ratio of liquid water mass to the total snow mass, $W = \rho_{w,sn}/\rho_{sn}$. To derive an equation for W , (1.11), first note that

$$W' = \frac{\rho'_{w,sn}}{\rho_{sn}} - \frac{W \rho'_{sn}}{\rho_{sn}}, \quad (\text{B.1})$$

where the primes denote time derivative, for brevity. The local mass balance of liquid water is governed by gravitational infiltration, γ_v , $[\gamma_v] = m/s$, and by the rate of freezing, F_{fr}^* :

$$\frac{\partial \rho_{w,sn}}{\partial t} = -\frac{\gamma_v \rho_{w0}}{\partial z} - F_{fr}^*, \quad (\text{B.2})$$

where we introduced the reference liquid water density, ρ_{w0} , to convert the volumetric flux to mass flux. In turn, the snow density is determined by gravitational water flux, and by the snow compaction, C_{sn} :

$$\frac{\partial \rho_{sn}}{\partial t} = -\frac{\gamma_v \rho_{w0}}{\partial z} + C_{sn}. \quad (\text{B.3})$$

Inserting (B.3) and (B.2) in (B.1) yeilds (1.11).